Measurement of the tau lepton lifetime

D. Buskulic, D. Casper, I. De Bonis, D. Decamp, P. Ghez, C. Goy, J.P. Lees, A. Lucotte, M.N. Minard, P. Odier, et al.

EUROPEAN LABORATORY FOR PARTICLE PHYSICS

CERN–PPE/95–128
22 August 1995

Measurement of the τ lepton lifetime

The ALEPH Collaboration[‡]

Abstract

The mean lifetime of the τ lepton is measured in a sample of 25700 τ pairs collected in 1992 with the ALEPH detector at LEP. A new analysis of the 1-1 topology events is introduced. In this analysis, the dependence of the impact parameter sum distribution on the daughter track momenta is taken into account, yielding improved precision compared to other impact parameter sum methods. Three other analyses of the one- and three-prong τ decays are updated with increased statistics. The measured lifetime is $293.5 \pm 3.1 \pm 1.7\,\mathrm{fs}$. Including previous (1989–1991) ALEPH measurements, the combined τ lifetime is $293.7 \pm 2.7 \pm 1.6\,\mathrm{fs}$.

(Submitted to Physics Letters B)

[‡]See the following pages for the list of authors.

The ALEPH Collaboration

D. Buskulic, D. Casper, I. De Bonis, D. Decamp, P. Ghez, C. Goy, J.-P. Lees, A. Lucotte, M.-N. Minard, P. Odier, B. Pietrzyk

Laboratoire de Physique des Particules (LAPP), IN^{2}P^3-CNRS, 74019 Annecy-le-Vieux Cedex, France

F. Ariztizabal, M. Chmeissani, J.M. Crespo, I. Efthymiopoulos, E. Fernandez, M. Fernandez-Bosman, V. Gaitan, Ll. Garrido,[15] M. Martinez, S. Orteu, A. Pacheco, C. Padilla, F. Palla, A. Pascual, J.A. Perlas, F. Sanchez, F. Teubert

Institut de Fisica d'Altes Energies, Universitat Autonoma de Barcelona, 08193 Bellaterra (Barcelona), Spain[7]

A. Colaleo, D. Creanza, M. de Palma, A. Farilla, G. Gelao, M. Girone, G. Iaselli, G. Maggi,[3] M. Maggi, N. Marinelli, S. Natali, S. Nuzzo, A. Ranieri, G. Raso, F. Romano, F. Ruggieri, G. Selvaggi, L. Silvestris, P. Tempesta, G. Zito

Dipartimento di Fisica, INFN Sezione di Bari, 70126 Bari, Italy

X. Huang, J. Lin, Q. Ouyang, T. Wang, Y. Xie, R. Xu, S. Xue, J. Zhang, L. Zhang, W. Zhao

Institute of High-Energy Physics, Academia Sinica, Beijing, The People's Republic of China[8]

G. Bonvicini, M. Cattaneo, P. Comas, P. Coyle, H. Drevermann, A. Engelhardt, R.W. Forty, M. Frank, R. Hagelberg, J. Harvey, R. Jacobsen,[24] P. Janot, B. Jost, E. Kneringer, J. Knobloch, I. Lehraus, C. Markou,[23] E.B. Martin, P. Mato, A. Minten, R. Miquel, T. Oest, P. Palazzi, J.R. Pater,[27] J.-F. Pusztaszeri, F. Ranjard, P. Rensing, L. Rolandi, D. Schlatter, M. Schmelling, O. Schneider, W. Tejessy, I.R. Tomalin, A. Venturi, H. Wachsmuth, W. Wiedenmann, T. Wildish, W. Witzeling, J. Wotschack

European Laboratory for Particle Physics (CERN), 1211 Geneva 23, Switzerland

Z. Ajaltouni, M. Bardadin-Otwinowska,[2] A. Barres, C. Boyer, A. Falvard, P. Gay, C. Guicheney, P. Henrard, J. Jousset, B. Michel, S. Monteil, J-C. Montret, D. Pallin, P. Perret, F. Podlyski, J. Proriol, J.-M. Rossignol, F. Saadi

Laboratoire de Physique Corpusculaire, Université Blaise Pascal, IN^{2}P^3-CNRS, Clermont-Ferrand, 63177 Aubière, France

T. Fearnley, J.B. Hansen, J.D. Hansen, J.R. Hansen, P.H. Hansen, B.S. Nilsson

Niels Bohr Institute, 2100 Copenhagen, Denmark[9]

A. Kyriakis, E. Simopoulou, I. Siotis, A. Vayaki, K. Zachariadou

Nuclear Research Center Demokritos (NRCD), Athens, Greece

A. Blondel,[21] G. Bonneaud, J.C. Brient, P. Bourdon, L. Passalacqua, A. Rougé, M. Rumpf, R. Tanaka, A. Valassi,[6] M. Verderi, H. Videau

Laboratoire de Physique Nucléaire et des Hautes Energies, Ecole Polytechnique, IN^{2}P^3-CNRS, 91128 Palaiseau Cedex, France

D.J. Candlin, M.I. Parsons

Department of Physics, University of Edinburgh, Edinburgh EH9 3JZ, United Kingdom[10]

E. Focardi, G. Parrini

Dipartimento di Fisica, Università di Firenze, INFN Sezione di Firenze, 50125 Firenze, Italy

M. Corden, M. Delfino,[12] C. Georgiopoulos, D.E. Jaffe

Supercomputer Computations Research Institute, Florida State University, Tallahassee, FL 32306-4052, USA [13,14]

A. Antonelli, G. Bencivenni, G. Bologna,[4] F. Bossi, P. Campana, G. Capon, V. Chiarella, G. Felici, P. Laurelli, G. Mannocchi,[5] F. Murtas, G.P. Murtas, M. Pepe-Altarelli

Laboratori Nazionali dell'INFN (LNF-INFN), 00044 Frascati, Italy

S.J. Dorris, A.W. Halley, I. ten Have,[6] I.G. Knowles, J.G. Lynch, W.T. Morton, V. O'Shea, C. Raine, P. Reeves, J.M. Scarr, K. Smith, M.G. Smith, A.S. Thompson, F. Thomson, S. Thorn, R.M. Turnbull

Department of Physics and Astronomy, University of Glasgow, Glasgow G12 8QQ,United Kingdom[10]

U. Becker, O. Braun, C. Geweniger, G. Graefe, P. Hanke, V. Hepp, E.E. Kluge, A. Putzer, B. Rensch, M. Schmidt, J. Sommer, H. Stenzel, K. Tittel, S. Werner, M. Wunsch

Institut für Hochenergiephysik, Universität Heidelberg, 69120 Heidelberg, Fed. Rep. of Germany[16]

R. Beuselinck, D.M. Binnie, W. Cameron, D.J. Colling, P.J. Dornan, N. Konstantinidis, L. Moneta, A. Moutoussi, J. Nash, G. San Martin, J.K. Sedgbeer, A.M. Stacey

Department of Physics, Imperial College, London SW7 2BZ, United Kingdom[10]

G. Dissertori, P. Girtler, D. Kuhn, G. Rudolph

Institut für Experimentalphysik, Universität Innsbruck, 6020 Innsbruck, Austria[18]

C.K. Bowdery, T.J. Brodbeck, P. Colrain, G. Crawford, A.J. Finch, F. Foster, G. Hughes, T. Sloan, E.P. Whelan, M.I. Williams

Department of Physics, University of Lancaster, Lancaster LA1 4YB, United Kingdom[10]

A. Galla, A.M. Greene, K. Kleinknecht, G. Quast, J. Raab, B. Renk, H.-G. Sander, R. Wanke, P. van Gemmeren C. Zeitnitz

Institut für Physik, Universität Mainz, 55099 Mainz, Fed. Rep. of Germany[16]

J.J. Aubert, A.M. Bencheikh, C. Benchouk, A. Bonissent,[21] G. Bujosa, D. Calvet, J. Carr, C. Diaconu, F. Etienne, M. Thulasidas, D. Nicod, P. Payre, D. Rousseau, M. Talby

Centre de Physique des Particules, Faculté des Sciences de Luminy, IN^{2}P^3-CNRS, 13288 Marseille, France

I. Abt, R. Assmann, C. Bauer, W. Blum, D. Brown,[24] H. Dietl, F. Dydak,[21] G. Ganis, C. Gotzhein, K. Jakobs, H. Kroha, G. Lütjens, G. Lutz, W. Männer, H.-G. Moser, R. Richter, A. Rosado-Schlosser, S. Schael, R. Settles, H. Seywerd, R. St. Denis, G. Wolf

Max-Planck-Institut für Physik, Werner-Heisenberg-Institut, 80805 München, Fed. Rep. of Germany[16]

R. Alemany, J. Boucrot, O. Callot, A. Cordier, F. Courault, M. Davier, L. Duflot, J.-F. Grivaz, Ph. Heusse, M. Jacquet, D.W. Kim,[19] F. Le Diberder, J. Lefrançois, A.-M. Lutz, G. Musolino, I. Nikolic, H.J. Park, I.C. Park, M.-H. Schune, S. Simion, J.-J. Veillet, I. Videau

Laboratoire de l'Accélérateur Linéaire, Université de Paris-Sud, IN^{2}P^3-CNRS, 91405 Orsay Cedex, France

D. Abbaneo, P. Azzurri, G. Bagliesi, G. Batignani, S. Bettarini, C. Bozzi, G. Calderini, M. Carpinelli, M.A. Ciocci, V. Ciulli, R. Dell'Orso, R. Fantechi, I. Ferrante, F. Fidecaro, L. Foà,[1] F. Forti, A. Giassi, M.A. Giorgi, A. Gregorio, F. Ligabue, A. Lusiani, P.S. Marrocchesi, A. Messineo, G. Rizzo, G. Sanguinetti, A. Sciabà, P. Spagnolo, J. Steinberger, R. Tenchini, G. Tonelli,[26] G. Triggiani, C. Vannini, P.G. Verdini, J. Walsh

Dipartimento di Fisica dell'Università, INFN Sezione di Pisa, e Scuola Normale Superiore, 56010 Pisa, Italy

A.P. Betteridge, G.A. Blair, L.M. Bryant, F. Cerutti, Y. Gao, M.G. Green, D.L. Johnson, T. Medcalf, Ll.M. Mir, P. Perrodo, J.A. Strong

Department of Physics, Royal Holloway & Bedford New College, University of London, Surrey TW20 OEX, United Kingdom[10]

V. Bertin, D.R. Botterill, R.W. Clifft, T.R. Edgecock, S. Haywood, M. Edwards, P. Maley, P.R. Norton, J.C. Thompson

Particle Physics Dept., Rutherford Appleton Laboratory, Chilton, Didcot, Oxon OX11 OQX, United Kingdom[10]

B. Bloch-Devaux, P. Colas, S. Emery, W. Kozanecki, E. Lançon, M.C. Lemaire, E. Locci, B. Marx, P. Perez, J. Rander, J.-F. Renardy, A. Roussarie, J.-P. Schuller, J. Schwindling, A. Trabelsi, B. Vallage

CEA, DAPNIA/Service de Physique des Particules, CE-Saclay, 91191 Gif-sur-Yvette Cedex, France[17]

R.P. Johnson, H.Y. Kim, A.M. Litke, M.A. McNeil, G. Taylor

Institute for Particle Physics, University of California at Santa Cruz, Santa Cruz, CA 95064, USA[22]

A. Beddall, C.N. Booth, R. Boswell, S. Cartwright, F. Combley, I. Dawson, A. Koksal, M. Letho, W.M. Newton, C. Rankin, L.F. Thompson

Department of Physics, University of Sheffield, Sheffield S3 7RH, United Kingdom[10]

A. Böhrer, S. Brandt, G. Cowan, E. Feigl, C. Grupen, G. Lutters, J. Minguet-Rodriguez, F. Rivera,[25] P. Saraiva, L. Smolik, F. Stephan,

Fachbereich Physik, Universität Siegen, 57068 Siegen, Fed. Rep. of Germany[16]

M. Apollonio, L. Bosisio, R. Della Marina, G. Giannini, B. Gobbo, F. Ragusa[20]

Dipartimento di Fisica, Università di Trieste e INFN Sezione di Trieste, 34127 Trieste, Italy

J. Rothberg, S. Wasserbaech

Experimental Elementary Particle Physics, University of Washington, WA 98195 Seattle, U.S.A.

S.R. Armstrong, L. Bellantoni,[30] P. Elmer, Z. Feng, D.P.S. Ferguson, Y.S. Gao, S. González, J. Grahl, J.L. Harton,[28] O.J. Hayes, H. Hu, P.A. McNamara III, J.M. Nachtman, W. Orejudos, Y.B. Pan, Y. Saadi, M. Schmitt, I.J. Scott, V. Sharma,[29] J.D. Turk, A.M. Walsh, Sau Lan Wu, X. Wu, J.M. Yamartino, M. Zheng, G. Zobernig

Department of Physics, University of Wisconsin, Madison, WI 53706, USA[11]

---

[1] Now at CERN, 1211 Geneva 23, Switzerland.
[2] Deceased.
[3] Now at Dipartimento di Fisica, Università di Lecce, 73100 Lecce, Italy.
[4] Also Istituto di Fisica Generale, Università di Torino, Torino, Italy.
[5] Also Istituto di Cosmo-Geofisica del C.N.R., Torino, Italy.
[6] Supported by the Commission of the European Communities, contract ERBCHBICT941234.
[7] Supported by CICYT, Spain.
[8] Supported by the National Science Foundation of China.
[9] Supported by the Danish Natural Science Research Council.
[10] Supported by the UK Particle Physics and Astronomy Research Council.
[11] Supported by the US Department of Energy, grant DE-FG0295-ER40896.
[12] On leave from Universitat Autonoma de Barcelona, Barcelona, Spain.
[13] Supported by the US Department of Energy, contract DE-FG05-92ER40742.
[14] Supported by the US Department of Energy, contract DE-FC05-85ER250000.
[15] Permanent address: Universitat de Barcelona, 08208 Barcelona, Spain.
[16] Supported by the Bundesministerium für Forschung und Technologie, Fed. Rep. of Germany.
[17] Supported by the Direction des Sciences de la Matière, C.E.A.
[18] Supported by Fonds zur Förderung der wissenschaftlichen Forschung, Austria.
[19] Permanent address: Kangnung National University, Kangnung, Korea.
[20] Now at Dipartimento di Fisica, Università di Milano, Milano, Italy.
[21] Also at CERN, 1211 Geneva 23, Switzerland.
[22] Supported by the US Department of Energy, grant DE-FG03-92ER40689.
[23] Now at University of Athens, 157-71 Athens, Greece.
[24] Now at Lawrence Berkeley Laboratory, Berkeley, CA 94720, USA.
[25] Partially supported by Colciencias, Colombia.
[26] Also at Istituto di Matematica e Fisica, Università di Sassari, Sassari, Italy.
[27] Now at Schuster Laboratory, University of Manchester, Manchester M13 9PL, UK.
[28] Now at Colorado State University, Fort Collins, CO 80523, USA.
[29] Now at University of California at San Diego, La Jolla, CA 92093, USA.
[30] Now at Fermi National Accelerator Laboratory, Batavia, IL 60510, USA.

1 Introduction

The first theoretical descriptions of the weak interactions were motivated by the observation that muon decay, muon capture, and neutron decay are all roughly characterized by a single coupling constant. The universality of the charged-current coupling is incorporated in the standard model of electroweak interactions. The hypothesis of lepton universality may be tested by comparing the decay rates of[1] $\tau^- \to e^-\nu\bar{\nu}$, $\tau^- \to \mu^-\nu\bar{\nu}$, and $\mu^- \to e^-\nu\bar{\nu}$. With the possibility of a different coupling constant g_ℓ for each lepton generation, the universality tests may be written

$$\left(\frac{g_\mu}{g_e}\right)^2 = \frac{B(\tau \to \mu\nu\bar{\nu})}{B(\tau \to e\nu\bar{\nu})}\frac{f(m_e^2/m_\tau^2)}{f(m_\mu^2/m_\tau^2)}, \tag{1}$$

$$\left(\frac{g_\tau}{g_\mu}\right)^2 = B(\tau \to e\nu\bar{\nu})\frac{\tau_\mu}{\tau_\tau}\left(\frac{m_\mu}{m_\tau}\right)^5\frac{f(m_e^2/m_\mu^2)}{f(m_e^2/m_\tau^2)}\Delta_{\rm W}\,\Delta_\gamma, \tag{2}$$

$$\left(\frac{g_\tau}{g_e}\right)^2 = B(\tau \to \mu\nu\bar{\nu})\frac{\tau_\mu}{\tau_\tau}\left(\frac{m_\mu}{m_\tau}\right)^5\frac{f(m_e^2/m_\mu^2)}{f(m_\mu^2/m_\tau^2)}\Delta_{\rm W}\,\Delta_\gamma, \tag{3}$$

where $f(x) = 1 - 8x + 8x^3 - x^4 - 12x^2\ln x$ is a correction for the masses of the charged leptons, $\Delta_{\rm W} = 0.9997$ is a correction to the W propagator, and $\Delta_\gamma = 1.0001$ is a QED radiative correction [1].

Non-universal effective couplings may arise from direct violation of lepton universality or from other extensions of the Standard Model [2]. At present, the sensitivity of the universality tests is limited by the experimental uncertainties on the τ lifetime and branching fractions. In this letter, an improved measurement of the τ lifetime is presented. Four analysis methods are used. The first, the momentum-dependent impact parameter sum method (MIPS), is a new method for analyzing the 1-1 topology events in which the mean lifetime is extracted from the impact parameter sum distribution. The impact parameter sum is, roughly speaking, the distance between the two daughter tracks at their point of closest approach to the beam axis. The strong dependence of the impact parameter sum distribution on the daughter track momenta is taken into account in this analysis. The other three measurements reported herein are updates based on the impact parameter sum (IPS), impact parameter difference (IPD), and decay length (DL) methods [3, 4].

The MIPS and IPS measurements have small statistical uncertainties because the impact parameter smearing related to the size of the luminous region is nearly cancelled in the impact parameter sum. These results are, however, sensitive to the assumed impact parameter resolution. On the other hand, the IPD method, also applied to 1-1 events, is subject to a statistical error from the size of the luminous region, but the fitting procedure used to determine the lifetime is insensitive to the impact parameter resolution. The DL method yields a precise lifetime measurement from τ's decaying into three-prong final states.

In the following, the impact parameter of a reconstructed daughter track with respect to the beam axis is denoted d. The impact parameter is measured in the projection onto the plane perpendicular to the beam axis. By convention, the sign of d is chosen to be that of the z component of the particle's angular momentum about the beam axis. In the case of perfect resolution and zero beam size, the impact parameter of a daughter track

[1] Decays with final state photons are implicitly included.

is related to the τ decay length ℓ according to

$$d = \ell \sin\theta \sin\psi, \tag{4}$$

where θ is the angle between the τ momentum and the incident e^- beam, and ψ is the signed azimuthal angle between the daughter track and the parent τ. In a 1-1 event, the sum of the impact parameters, $d_+ + d_-$, is denoted δ.

A τ mass of $m_\tau = 1776.96 \pm 0.26\,\mathrm{MeV}/c^2$ [5] is assumed throughout this paper.

2 Apparatus and data sample

The ALEPH detector is described in detail elsewhere [6, 7]. The tracking system consists of a high-resolution silicon strip vertex detector (VDET), a cylindrical drift chamber (the inner tracking chamber or ITC), and a large time projection chamber (TPC). The VDET features two layers of 300 μm thick silicon wafers. Each layer provides measurements in both the r-ϕ and r-z views at average radii of 6.3 and 10.8 cm. The spatial resolution for r-ϕ coordinates is 12 μm and varies between 12 and 22 μm for z coordinates, depending on track polar angle. The angular coverage is $|\cos\theta| < 0.85$ for the inner layer and $|\cos\theta| < 0.69$ for the outer layer. The design of VDET includes a 5% overlap of the active regions of adjacent wafers in r-ϕ, providing a constraint on the circumferences of the VDET layers through studies of reconstructed charged tracks. In this situation, the overall scale of measured impact parameters and decay lengths is essentially set by the average pitch of the strips on the VDET wafers, which is known with a relative uncertainty of less than 10^{-4}. The ITC has eight coaxial wire layers at radii of 16 to 26 cm. The TPC provides up to 21 three-dimensional coordinates per track at radii between 40 and 171 cm. A superconducting solenoid produces a magnetic field of 1.5 T.

Charged tracks measured in the VDET-ITC-TPC system are reconstructed with a momentum resolution of $\Delta p/p = 6 \times 10^{-4} p_T\,(\mathrm{GeV}/c)^{-1} \oplus 0.005$. An impact parameter resolution of 28 μm in the r-ϕ plane is achieved for muons from $\mathrm{Z} \to \mu^+\mu^-$ having at least one VDET r-ϕ hit.

The electromagnetic calorimeter (ECAL) is a lead/wire-chamber sandwich operated in proportional mode. The calorimeter is read out via projective towers subtending typically $0.9^\circ \times 0.9^\circ$ in solid angle which sum the deposited energy in three sections in depth. The hadron calorimeter (HCAL) uses the iron return yoke as absorber with an average depth of 1.50 m. Hadronic showers are sampled by 23 planes of streamer tubes, providing a digital hit pattern and inducing an analog signal on pads arranged in projective towers. The HCAL is used in combination with two layers of muon chambers outside the magnet for μ identification.

The data sample used in this analysis was collected in 1992 at $\sqrt{s} = 91.3$ GeV and corresponds to 32100 produced τ pairs. Candidate τ-pair events are selected according to the algorithm described in [8]. The overall efficiency for this selection is 78%, with an expected background contamination of 1.6%. The $\tau^+\tau^-$ sample contains 25679 candidate events to which further cuts are applied for the different analyses.

Table 1: Numbers of surviving candidate events in the 1-1 event selection.

Cut	Events
$\tau^+\tau^-$ candidates	25679
1-1 topology	14808
Opposite charges	14611
$\lvert d_\pm\rvert < 2\,\mathrm{cm}$; $\lvert z_\pm\rvert < 10\,\mathrm{cm}$	14599
Bhabha rejection	14363
≤ 2 extra tracks	13939
≥ 1 VDET r-ϕ hit	13219
≥ 4 ITC hits	12934
≥ 8 TPC hits	12876
Track fit $\chi^2/\mathrm{dof} < 5$	12485
$p > 1\,\mathrm{GeV}/c$	12096
Bremsstrahlung rejection	11494
Final state radiation rejection	10983

3 Selection of 1-1 topology events

Three different analyses of the 1-1 topology events are described in sections 5, 6, and 7. Each event in the basic $\tau^+\tau^-$ sample is divided into hemispheres according to the reconstructed thrust axis. The 1-1 events are selected by requiring each hemisphere to contain exactly one track with VDET hits. The two tracks are required to have opposite charges and satisfy very loose cuts on $d_\pm$ and $z_\pm$ (the z coordinate at the point of closest approach to the beam axis). Up to two extra tracks (without VDET hits), *e.g.,* from photon conversion, are allowed in each hemisphere. Additional track quality cuts are imposed to ensure that the τ daughter tracks are well measured. Information from the ECAL is used to reject electrons from $\tau \to e\nu\bar{\nu}$ decays that undergo hard bremsstrahlung in the detector material. When evidence of a bremsstrahlung photon is found, either as a separated cluster in the ECAL or in the form of excess energy in the electron cluster, the expected impact parameter shift due to the bremsstrahlung interaction, Δd, is estimated. This estimate is independent of the actual reconstructed impact parameter. The event is rejected if $|\Delta d| > 100\,\mu\mathrm{m}$. Finally, events with hard final state radiation are rejected by requiring both hemisphere invariant masses to be less than $2\,\mathrm{GeV}/c^2$. The mass is computed from the charged daughter track (assumed to be a pion) and all photon candidates with energy greater than 2 GeV. The selection criteria for 1-1 events are summarized in table 1. The selection algorithm is more efficient and rejects more background than the scheme used in [4]. The efficiency for selecting $\tau^+\tau^-$ events of 1-1 topology is 47%. Monte Carlo simulations of $e^+e^- \to e^+e^-$, $\mu^+\mu^-$, $q\bar{q}$, and $\gamma\gamma \to \ell^+\ell^-$, $q\bar{q}$ are used to predict the background contamination in the 1-1 sample, $0.37 \pm 0.05(\mathrm{stat})\%$. The dominant background source is the reaction $\gamma\gamma \to \ell^+\ell^-$. The contamination from cosmic rays is of the order of 0.01%.

4 Impact parameter sum resolution

Both the MIPS analysis (section 5) and the IPS analysis (section 6) require an accurate evaluation of the impact parameter sum resolution for each event of 1-1 topology. The rms resolution on the impact parameter sum is 80 μm, compared to 180 μm for the rms of the true impact parameter sum distribution in the selected $\tau^+\tau^-$ events. A parametrization of the resolution, based on measurements from real e^+e^- and $\mu^+\mu^-$ events and simulated $\tau^+\tau^-$ events, is described in this section.

The resolution function is written as the convolution of three terms:

$$g(\delta - \delta') = R_+ \otimes R_- \otimes G(\sigma_{\rm b}), \tag{5}$$

where δ' denotes the true impact parameter sum with respect to the $\tau^+\tau^-$ production point and R_+ and R_- describe the measurement error distribution for the two impact parameters, d_+ and d_-. $G(\sigma_{\rm b})$ represents a small additional smearing related to the size of the interaction region. This smearing arises because the impact parameters are measured with respect to the beam axis rather than the $\tau^+\tau^-$ production point.

The tracking resolution function for each impact parameter is taken to be the sum of three Gaussian functions:

$$R_\pm = (1 - a_2 - a_3)G(\sigma) + a_2 G(b_2\sigma) + a_3 G(b_3\sigma). \tag{6}$$

The parameter σ represents the width of the Gaussian resolution core, while a_2, b_2, a_3, and b_3 characterize the amplitudes and widths of the second and third Gaussian functions which describe the tails of the distribution.

Measurement of the impact parameter sum for track pairs having a common spatial origin offers direct experimental access to the actual tracking resolution function R. To cover the entire relevant momentum range, e^+e^- and $\mu^+\mu^-$ final states coming from Z decays and $\gamma\gamma$ collisions are analyzed. The impact parameter resolution is measured separately for the electron and muon samples. Another set of resolution parameters is extracted from simulated $\mathrm{Z} \to \tau^+\tau^-$ events.

It is assumed that the resolution for a given track depends on the error estimate $\hat{\sigma}$ provided by the track helix fitter, the track momentum p, the polar angle θ, and the configuration of vertex detector r-ϕ hits (hit in the inner layer only, outer layer only, or both layers).

The width of the Gaussian core of the tracking resolution, σ, is derived from the track fit error $\hat{\sigma}$ in the following way. First, the error estimate $\hat{\sigma}$ is parametrized by the function $\hat{s}_k(p,\theta)$, where

$$\hat{s}_k^2(p,\theta) = \hat{\sigma}_{{\rm int},k}^2 + \frac{\hat{\sigma}_{{\rm ms},k}^2}{p^2 \sin^3\theta}, \tag{7}$$

and $k = 1,2,3$ identifies the VDET hit configuration. The parameters $\hat{\sigma}_{{\rm int},k}$ and $\hat{\sigma}_{{\rm ms},k}$ are extracted by means of a fit to the $\hat{\sigma}$ values; $\hat{\sigma}_{{\rm int},k}$ describes the intrinsic detector resolution, $\hat{\sigma}_{{\rm ms},k}$ the contribution of the multiple scattering. The angular dependence corresponds to scattering of straight tracks by cylindrical shells of material.

The parameters of the resolution function R are then determined by means of a fit to

the reconstructed impact parameter sum distribution, under the assumption that

$$\sigma = \hat{\sigma}\,\frac{s_k(p,\theta)}{\hat{s}_k(p,\theta)}, \tag{8}$$

where $s_k(p,\theta)$ has the same functional form as $\hat{s}_k(p,\theta)$. This second fit measures the parameters $\sigma_{\mathrm{int},k}$ and $\sigma_{\mathrm{ms},k}$ which correspond to the observed detector intrinsic resolution and multiple scattering term.

Other parameters are also left free to vary in this second fit. The amplitude of the second Gaussian function, a_2, is allowed to depend on the track momentum according to the empirical formula

$$a_2 = \frac{a_{\mathrm{high}}p^2 + a_{\mathrm{low}}\,p_{\mathrm{min}}\,p_{\mathrm{max}}}{p^2 + p_{\mathrm{min}}\,p_{\mathrm{max}}}. \tag{9}$$

The parameters a_{high} and a_{low} describe the asymptotic values of a_2 for high and low momentum tracks, respectively; $p_{\mathrm{min}} = 1\,\mathrm{GeV}/c$, $p_{\mathrm{max}} = 45\,\mathrm{GeV}/c$. The width of the second Gaussian, on the other hand, is fixed to $b_2 = 3$ times the core width, a value that fits the impact parameter resolution of all the selected data samples reasonably well. The systematic effects of this choice are estimated by varying b_2 by 20% of its value. Finally, the parameters a_3 and b_3 are left free to match the more distant tails of the tracking resolution.

The τ daughter tracks studied in the lifetime analyses are electrons, muons, and hadrons. An average resolution function for the one-prong τ decays is assembled from the parameters obtained from the real e^+e^- and $\mu^+\mu^-$ events and simulated $\tau^+\tau^-$ events. The parameters of the first and second Gaussians in the d resolution function for high momentum electrons differ significantly from the muon parameters, whereas these parameters are comparable for muons and hadrons in simulated τ decays. The resolution function used in the lifetime fit to the data is therefore constructed by combining the electron and muon parameters for the first and second Gaussians in proportion to the electron abundance in τ decays. Hadron tracks contribute most to the far tails of the tracking resolution in Monte Carlo τ decays. Large tracking errors may result either from nuclear interactions or from confusion caused by extra tracks produced in photon conversions. The parameters a_3 and b_3 used to describe the long resolution tails in the lifetime fits are thus taken from the $\tau^+\tau^-$ Monte Carlo sample. The second Gaussian contains between 5% and 12% of the tracks, depending on momentum. The third Gaussian contains roughly 0.2% of the tracks; its width is about 20 times that of the core Gaussian.

The entire procedure is repeated for simulated e^+e^- and $\mu^+\mu^-$ events. Background events (mostly from $\mathrm{Z} \to \tau^+\tau^-$ and $\gamma\gamma \to \tau^+\tau^-$) are included in the Monte Carlo analysis. The resolution parameters so obtained are used to study the lifetime analysis methods with simulated $\tau^+\tau^-$ events.

An important source of systematic uncertainty in the lifetime analyses is the simulation accuracy for hadron tracks, which is assessed in a study of real and simulated $e^+e^- \to q\bar{q}$ events. The resolution is measured from the impact parameter distribution of hadron tracks whose reconstructed point of closest approach to the axis of their jet lies upstream of the primary vertex. The impact parameters are measured with respect to the primary vertex, which is reconstructed for each event. Non-Gaussian resolution tails are measured in three different momentum ranges, and for samples requiring either one or two vertex

detector hits. The contribution of lepton tracks to the far tails is studied by comparing the fitted values of a_3 and b_3 from the real and simulated e^+e^- and $\mu^+\mu^-$ samples.

Other contributions to the systematic uncertainty in the τ lifetime analyses are determined from the statistical uncertainties on the fitted resolution parameters. A possible difference between muons and hadrons is taken into account by inflating the statistical uncertainties on $a_{\rm high}$ and $a_{\rm low}$ according to the statistical precision of the comparison between Monte Carlo $\mu^+\mu^-$ events and hadronic τ decays.

In these resolution studies and in all three lifetime analyses of the 1-1 events, the reconstructed track impact parameters are corrected for systematic offsets due to detector alignment and drift field parametrization errors. The offsets are measured as a function of θ and ϕ from a large sample of tracks from $\mathrm{Z} \to q\bar{q}$ events. The d corrections are typically $15\,\mu$m.

The function $G(\sigma_{\rm b})$, which describes the smearing related to the beam size, is a Gaussian function with variance

$$\sigma_{\rm b}^2 = 4\sin^2\frac{\Delta\phi}{2}\,(\sigma_x^2\sin^2\overline{\phi} + \sigma_y^2\cos^2\overline{\phi}), \tag{10}$$

where σ_x and σ_y represent the rms width and height of the interaction region, $\Delta\phi = \phi_+ - \phi_- \pm \pi$ is the acollinearity of the tracks in the r-ϕ projection, and $\overline{\phi} = (\phi_+ + \phi_-)/2$. The beam axis position is determined from selected reconstructed charged tracks in Z decay events (excluding τ pairs), averaged over blocks of roughly 75 events. The vertical extent of the luminous region is taken to be $5\,\mu$m (rms). The horizontal extent of the luminous region (typically $110\,\mu$m rms) is measured from the fitted primary vertices of selected $\mathrm{Z} \to q\bar{q}$ decays, over blocks of about 270 events. The uncertainty on the position of the beam axis is folded into σ_x and σ_y.

5 Momentum-dependent impact parameter sum analysis

The MIPS method, a variation of the "miss distance" method [9], is applied to events of 1-1 topology. In this analysis, the momenta $p_\pm$ of the charged daughter tracks are used in addition to δ in a maximum likelihood fit for the mean τ lifetime. The daughter track momenta are strongly correlated with the τ decay angles. For monoenergetic τ's decaying into two bodies, there is a one-to-one relationship between the charged daughter momentum and the angle between the τ and daughter directions in three dimensions. The presence of three-body decays and final states with π^0's dilutes the correlation somewhat. Nevertheless, the width of the d distribution depends strongly on the charged daughter momentum, as shown in fig. 1. The plots show the mean of $|\hat{d}|/c\tau_{\rm mc}$ as a function of p in the accepted Monte Carlo events, where $\hat{d}$ denotes the true impact parameter with respect to the $\tau^+\tau^-$ production point and $\tau_{\rm mc}$ is the mean τ lifetime assumed in the Monte Carlo generator. The two plots correspond to the two possible "event helicities." The event helicity of a $\mathrm{Z} \to \tau^+\tau^-$ event is defined to be the helicity of the τ^-. The $\hat{d}$ distribution also depends slightly on the τ polar angle θ_τ; the plots in fig. 1 are integrated over θ_τ.

For a given p, the $\hat{d}$ distribution has a cusp at $\hat{d} = 0$ and is symmetric about that point. To construct the likelihood function it is necessary to parametrize the distribution

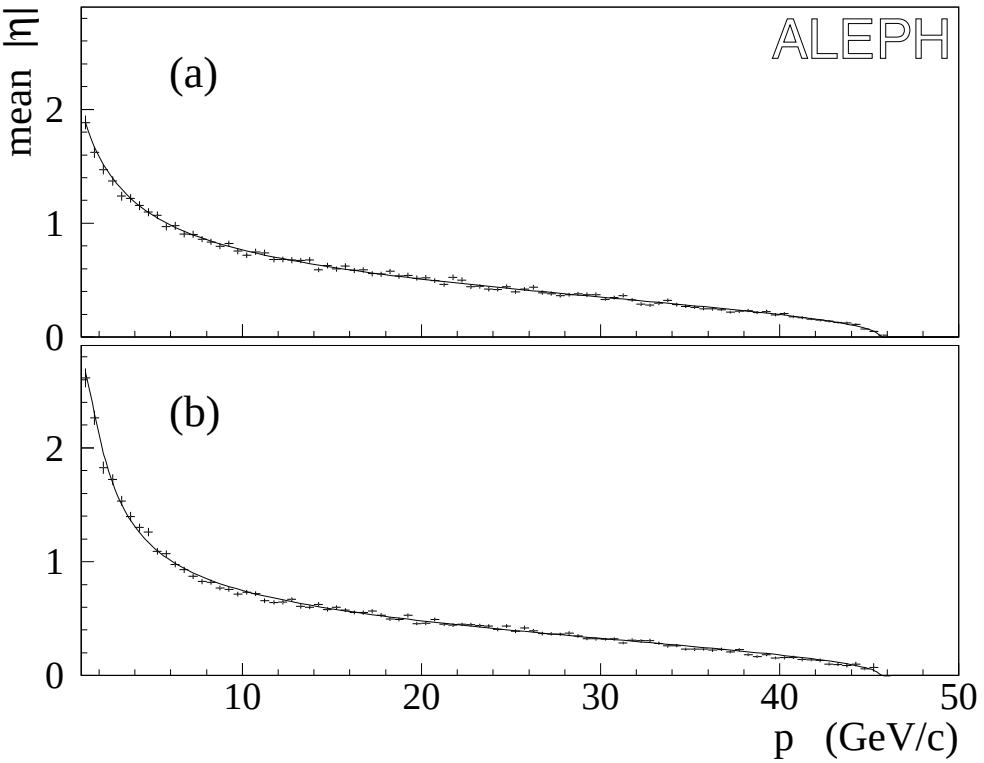

Figure 1: Mean of $|\eta| = |\hat{d}|/c\tau_{\rm mc}$ as a function of the daughter track momentum: (a) positive helicity events and (b) negative helicity events, as defined in the text. For a given event, the τ^+ and τ^- decays enter the same plot. The curves show the parametrization described in the text.

of $\hat{d}$ as a function of p and θ_τ. Since the true impact parameters are proportional to the τ lifetimes, the required information about τ decay angles and momenta is contained in the distribution of $\eta \equiv \hat{d}/c\tau_{\rm mc}$. The η probability density for event helicity h is well represented by the sum of two bipolar exponential functions:

$$f_h(\eta|p,\theta_\tau) = \frac{r}{2\lambda_1\lambda(p,\theta_\tau)} \exp\frac{-|\eta|}{\lambda_1\lambda(p,\theta_\tau)} \; + \; \frac{1-r}{2\lambda_2\lambda(p,\theta_\tau)} \exp\frac{-|\eta|}{\lambda_2\lambda(p,\theta_\tau)}, \tag{11}$$

with

$$\begin{aligned} r &= (\lambda_2 - 1)/(\lambda_2 - \lambda_1), \\ \lambda(p,\theta_\tau) &= (c_1 t + c_2 t^2 + c_3 t^3 + c_4 t^4 + c_5 t^5)(1 + c_6|\pi/2 - \theta_\tau|), \end{aligned} \tag{12}$$

and

$$t = \left(\frac{E_{\rm beam}}{pc} - 1\right)^{\frac{1}{2}}. \tag{13}$$

In this parametrization, $\lambda(p,\theta_\tau)$ is equal to the mean value of $|\eta|$ as a function of p and θ_τ. An independent set of parameters λ_1, λ_2, c_1, c_2, ..., c_6 is fitted for positive and negative event helicities. The curves plotted in fig. 1 represent the functions $\lambda(p,\theta_\tau)$, averaged over θ_τ.

The probability density function of $\Sigma\eta \equiv \eta_+ + \eta_-$ for fixed p_+, p_-, θ_τ, and event helicity h is then

$$\mathcal{E}_h(\Sigma\eta|p_+,p_-,\theta_\tau) = \int_{-\infty}^{\infty} d\eta_+ \int_{-\infty}^{\infty} d\eta_- f_h(\eta_+|p_+,\theta_\tau) f_h(\eta_-|p_-,\theta_\tau)\delta(\Sigma\eta - \eta_+ - \eta_-), \quad (14)$$

where θ_τ is now taken to be the polar angle of the τ^-, and δ is the Dirac delta function. Since the individual event helicities are unknown, the $\mathcal{E}_h$ are mixed according to the known τ polarization as a function of the τ^- polar angle:

$$\mathcal{E}(\Sigma\eta|p_+,p_-,\theta_\tau) = \frac{1+P_\tau(\theta_\tau)}{2}\mathcal{E}_+ \; + \; \frac{1-P_\tau(\theta_\tau)}{2}\mathcal{E}_-, \quad (15)$$

where

$$P_\tau(\theta_\tau) = -\frac{\mathcal{A}_\ell(1+\cos\theta_\tau)^2}{1+\cos^2\theta_\tau + 2\mathcal{A}_\ell^2\cos\theta_\tau} \quad (16)$$

at the Z peak. $\mathcal{A}_\ell$ is the measured asymmetry parameter [10]. The value of θ_τ is taken from the event thrust axis direction (computed from the reconstructed charged and neutral particles) in the hemisphere containing the τ^-. The uncertainty on the τ^- polar angle has an insignificant effect on the fitted lifetime.

The probability density function for the true impact parameter sum $\hat{\delta} = \hat{d}_+ + \hat{d}_-$ is

$$\mathcal{D}(\hat{\delta}|\tau_\tau,p_+,p_-,\theta_\tau) = \frac{1}{c\tau_\tau}\mathcal{E}(\hat{\delta}/c\tau_\tau|p_+,p_-,\theta_\tau). \quad (17)$$

The fitting function is constructed by convolving $\mathcal{D}$ with the resolution function described in section 4.

In order to remove the few remaining events with poorly measured tracks, a confidence level (CL) is calculated for each of the selected events. The CL of an event is defined to be the integrated probability density for the event to have a reconstructed δ equal to or larger than the observed value. (A mean τ lifetime of 296 fs is assumed for this calculation.) The CL distribution is found to be uniform, as expected, except for a peak at very small values. Since the 1-1 sample contains approximately 10^4 events, one event is expected to have CL $< 10^{-4}$; 8 such events are observed. These events are excluded from the fit, leaving a sample of 10975 events.

The fit to the data yields a mean τ lifetime of 297.1 ± 3.6 fs. Figure 2 shows the δ distribution for the data, overlayed with the best fit function.

Monte Carlo $\tau^+\tau^-$ events are used to check for biases in the analysis method. The lifetime fit yields $\tau_\tau = 297.8 \pm 1.1$ fs, compared with the input value, $\tau_{\rm mc} = 296$ fs. The calculated bias of $+0.61 \pm 0.38\%$ is subtracted from the lifetime value obtained from the data.

Additional systematic uncertainty on the measured lifetime arises from the parametrization of the impact parameter resolution and from the simulation of the τ decay distributions and the backgrounds. The uncertainty associated with the d resolution parametrization, $\pm 0.78\%$, includes contributions of $\pm 0.76\%$ from the statistical errors on the measured resolution parameters and $\pm 0.16\%$ from the parameters of the third Gaussian function, which are obtained from Monte Carlo events. A bias of $-0.07 \pm 0.07\%$ is related to the different η distributions for different τ decay modes; this value is based on the experimental uncertainties on the branching fractions and on a study of the efficiencies of the

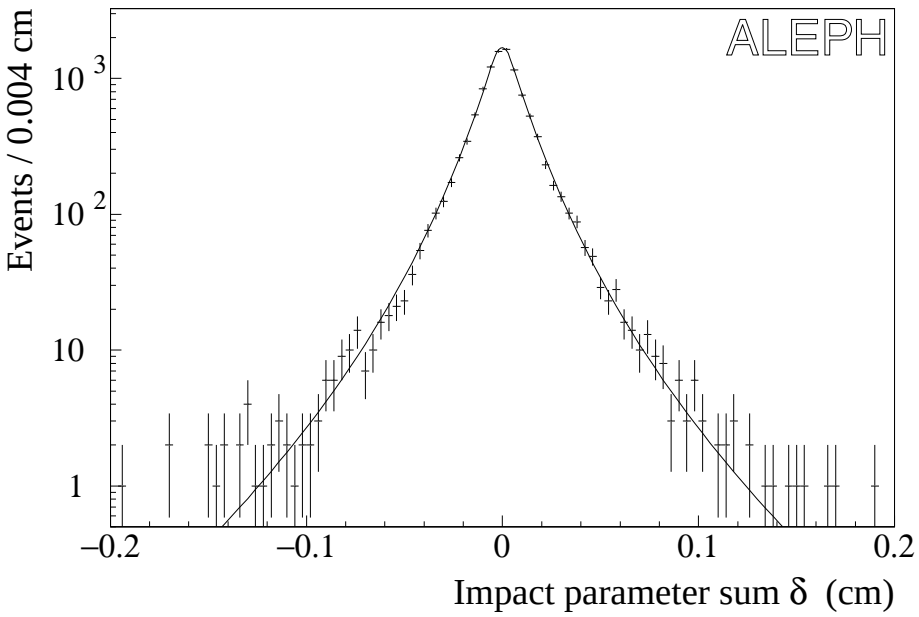

Figure 2: Impact parameter sum distribution for data. The overlayed curve is the result of the maximum likelihood fit.

event selection algorithm for the various decay modes in data and Monte Carlo. The correlation of the transverse polarizations of the τ^+ and τ^- is not simulated in the event generator [11] used for the final lifetime bias determination, so a special generator [12] without initial or final state radiation was used to determine that this correlation changes the measured lifetime by $-0.22 \pm 0.44\%$. The uncertainty associated with the longitudinal τ polarization is negligible. The bias due to background events is predicted from Monte Carlo simulation to be $-0.25 \pm 0.06\%$. The net bias is $+0.07\%$. The total systematic uncertainty of $\pm 0.97\%$ is the quadratic sum of the various contributions, including the statistical uncertainty on the Monte Carlo bias determination. The systematic uncertainties for all four τ lifetime analyses are summarized in table 2.

The mean τ lifetime obtained with the MIPS method, corrected for biases, is

$$\tau_\tau = 296.9 \pm 3.6\,(\text{stat}) \pm 2.9\,(\text{syst})\,\text{fs}. \tag{18}$$

6 Impact parameter sum analysis

The original IPS method [4] is also applied to the 1-1 event sample. In this analysis, the daughter track directions are considered in addition to the impact parameter sum in the fit for the mean τ lifetime. The sphericity axis is calculated for each event from the charged and neutral particles. The axis so obtained is used as an estimate of the τ production axis, from which the azimuthal τ decay angles $\psi_\pm$ are determined. The decay angles are defined as $\psi = \phi_{\text{daughter}} - \phi_\tau$.

The distribution of the true sum of impact parameters δ' may be expressed analytically

Table 2: Systematic uncertainties in the τ lifetime analyses. Dashes denote inapplicable or negligible contributions.

	Systematic uncertainties (%)			
Source	MIPS	IPS	IPD	DL
Monte Carlo statistics	0.38	0.41	0.32	0.61
d resolution measurement	0.76	0.97	–	–
d resolution simulation	0.16	0.12	0.26	–
Decay branching fractions/efficiencies	0.07	0.11	0.07	–
Transverse τ polarization correlation	0.44	0.44	–	–
Backgrounds	0.06	0.06	0.07	0.11
Detector alignment	–	–	0.10	0.36
Final state radiation	–	–	0.17	–
Vertex χ^2 cut	–	–	–	0.40
Total	0.97	1.15	0.47	0.82

in terms of the mean τ lifetime, for fixed θ, ψ'_+, and ψ'_- [4]. Here, θ denotes the polar angle of the τ^- momentum and $\psi'_\pm$ are the true decay angles. The measured $\psi_\pm$ angles are subject to correlated errors associated with the τ direction determination. These errors (typically 20 mrad in azimuth) are dominated by the effects of the unobserved neutrinos. Since the tracking errors on $\phi_\pm$ are negligible by comparison (typically 0.5 mrad), the resolution function for the reconstructed δ, ψ_+, and ψ_- may be factored into two independent functions g and h:

$$\frac{dN(\delta \,|\, \psi_+, \psi_-)}{d\delta} = \int d\psi'_+ \, d\psi'_- \, h(\psi_+, \psi_-, \psi'_+, \psi'_-) \int d\delta' \, g(\delta - \delta') \, \frac{dN(\delta' \,|\, \psi'_+, \psi'_-)}{d\delta'}. \qquad (19)$$

The resolution on the impact parameter sum is characterized by the function g, which is described in section 4. The function h gives the probability for a τ pair with reconstructed decay angles (ψ_+, ψ_-) to have true angles (ψ'_+, ψ'_-). This function is constructed numerically, averaging over track momenta and polar angles, in an analysis of a high statistics sample of simulated τ pairs without detector simulation.

Candidate τ pairs of 1-1 topology are first selected as described in section 3. Additional event selection requirements are imposed for this analysis. The requirement $|\psi| < 0.15$ rad reduces background from $\gamma\gamma$ processes and eliminates some of the remaining events that contain acoplanar τ's due to final state radiation. Finally, events containing mismeasured tracks are removed by the requirement $|\delta| < 0.18$ cm. A maximum likelihood fit is performed on the remaining 10464 events. The fitted mean τ decay length is $\langle \ell \rangle = 0.2231 \pm 0.0029$ cm. Figure 3 shows the distribution of δ for various ranges of $\psi_+ + \psi_-$. The fitted function is also shown.

A bias on the measured mean decay length is expected due to the use of the single (momentum-independent) h function. The correlated measurement errors on d and ψ are expected to yield a small positive decay length bias. Monte Carlo $\tau^+\tau^-$ events are analyzed in exactly the same way as the real events, in order to determine the total bias on the measured lifetime. The fitted mean decay length in the Monte Carlo sample is

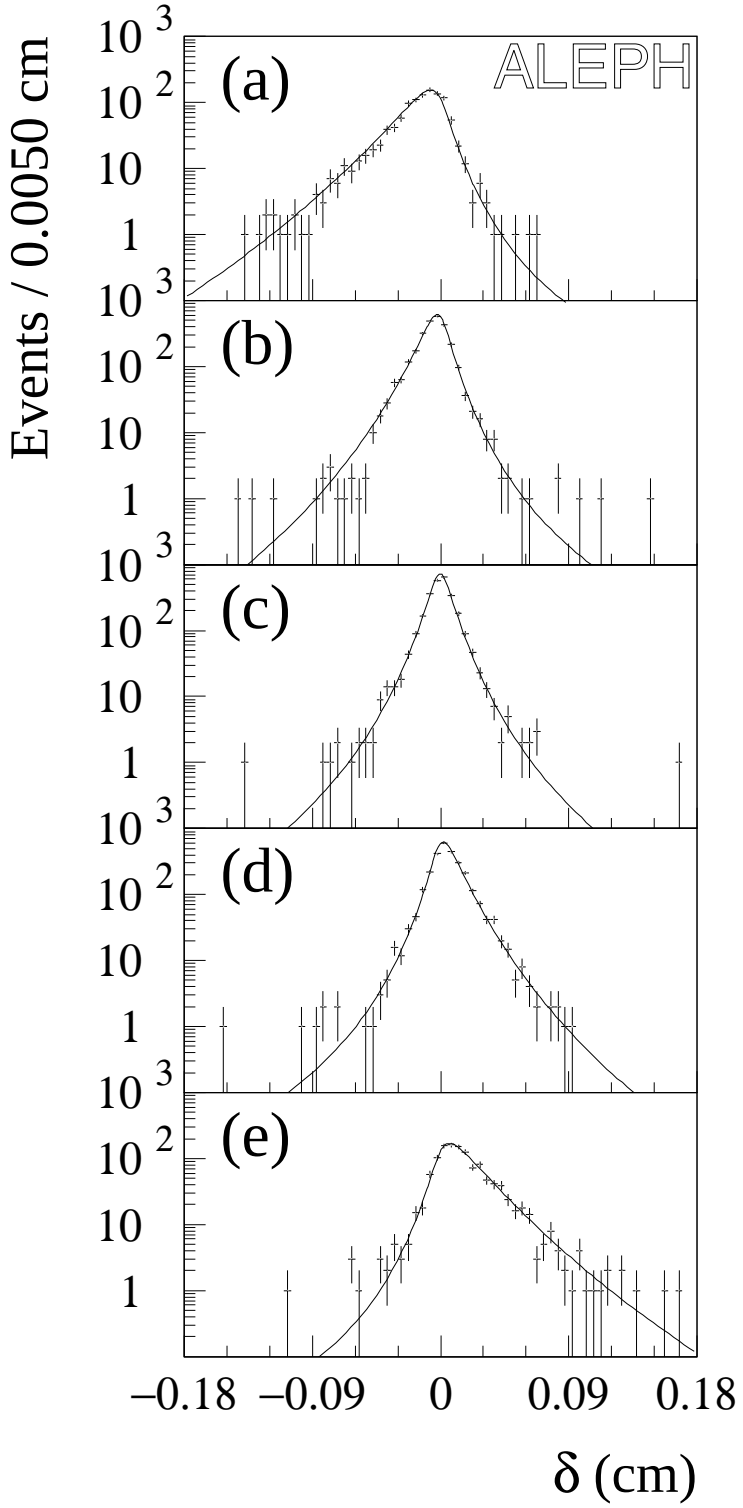

Figure 3: Impact parameter sum distribution for data, in various ranges of $S = \psi_+ + \psi_-$: (a) $S < -0.06$, (b) $-0.06 \leq S < -0.01$, (c) $-0.01 \leq S < 0.01$, (d) $0.01 \leq S < 0.06$, (e) $S \geq 0.06$. The curves are the results of the maximum likelihood fit.

$1.49 \pm 0.41\%$ lower than the generated value.

The other systematic uncertainties (table 2) are very similar to those described in section 5. The uncertainty associated with the measurement of the d resolution in data events is $\pm 0.97\%$. This includes contributions of $\pm 0.44\%$ for the parameters of the core Gaussian function and $\pm 0.86\%$ for the second Gaussian. A systematic uncertainty of $\pm 0.12\%$ is assigned for the parameters of the third Gaussian function. A bias of $-0.14 \pm 0.11\%$ is expected due to differences between data and Monte Carlo in the branching fractions and selection efficiencies for the various τ decay modes. The transverse τ polarization correlation gives a bias and uncertainty of $-0.22 \pm 0.44\%$. The bias due to background is $-0.24 \pm 0.06\%$. The total systematic bias and uncertainty is $-2.09 \pm 1.15\%$. After corrections, the mean τ lifetime obtained in the IPS analysis is

$$\tau_\tau = 297.4 \pm 3.8\,(\text{stat}) \pm 3.4\,(\text{syst})\,\text{fs}. \tag{20}$$

The systematic uncertainty related to the resolution parametrization is larger for IPS than for MIPS because the true impact parameter sum distribution assumed in the IPS fitting function has no explicit momentum dependence. In the MIPS analysis, tracks with lower momentum (and poorer resolution) are associated with a wider true impact parameter distribution, leading to a reduced sensitivity to the resolution parameters.

7 Impact parameter difference analysis

The 1-1 topology events were also analyzed with the IPD method. A brief description of this method is given here; more details are given in [3] and [4]. The following quantities are determined for each event:

$$\begin{aligned} Y &= d_+ - d_-, \\ X &= \frac{\bar{p}_\tau(\sqrt{s})}{\bar{p}^0_\tau}\,\Delta\phi\,\sin\theta, \end{aligned} \tag{21}$$

where $\bar{p}_\tau(\sqrt{s})$ is the mean τ momentum, determined from Monte Carlo simulation after all event selection criteria are applied, $\bar{p}^0_\tau$ is the mean τ momentum at $\sqrt{s} = 91.25\,\text{GeV}$, and θ is taken from the event thrust axis. No estimate of the τ direction is needed to determine $\Delta\phi$ $(= \phi_+ - \phi_- \pm \pi)$. The lifetime is then determined from the Y *vs.* X distribution and the relation

$$\langle Y \rangle \;=\; \left[\frac{\bar{p}^0_\tau}{m_\tau}\tau_\tau\right] X. \tag{22}$$

The parameters of the line $\langle Y \rangle = a_0 + a_1 X$ are determined by means of an unbinned, weighted least-squares fit with an iterative trimming procedure to remove poorly measured events.

The IPD analysis of the 1992 data benefits from the smaller LEP beam size and from an improved event selection algorithm (section 3) compared to the 1991 analysis. Another important change is the reduction of the trim fraction in the fit from 2% to 0.2% of the events. The new trim fraction is chosen to minimize the statistical and systematic uncertainty on the lifetime.

The fit range $|X| < 0.18$ is chosen in order to reduce the effect of radiative $\text{Z} \to \tau^+\tau^-$ events and background from two-photon interactions; 10876 events enter the fit. The fit

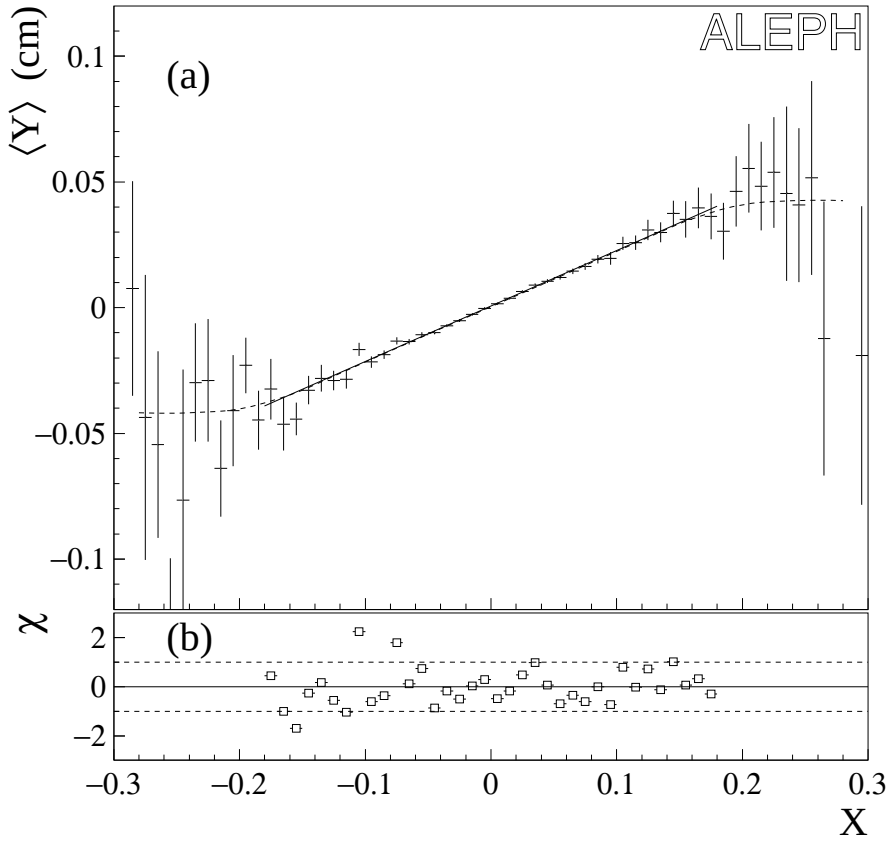

Figure 4: (a) $\langle Y \rangle$ *vs.* X. The solid line shows the result of the fit described in the text. The dashed curve shows the expected shape of $\langle Y \rangle$ *vs.* X. (b) Plot of pulls (deviation from fitted line divided by uncertainty).

results are $a_0 = +0.0004 \pm 0.0002\,\mathrm{cm}$ and $a_1 = +0.2204 \pm 0.0041\,\mathrm{cm}$, with $\chi^2 = 11500$ for 10853 degrees of freedom (fig. 4). From simulated events the intercept a_0 is predicted to be $+0.0003 \pm 0.0001\,\mathrm{cm}$; the offset from zero is caused by bremsstrahlung of daughter $e^{\pm}$ tracks in the detector material. As a check of the procedure, different fit ranges in X are used. The resulting variations in the fitted slope are consistent with those observed for Monte Carlo events.

The fitted value of a_1 is corrected for several biases which are estimated from Monte Carlo simulation. The lifetime bias introduced by the selection procedure is $+0.29 \pm 0.18\%$. Surviving radiative events tend to have shorter decay lengths and a wider X distribution. Although the lifetime calculation does take into account the reduction of the mean τ momentum due to radiation, the greater influence in the fit of events with large $|X|$ yields an additional bias of $-0.18 \pm 0.03\%$. The assumption that $\Delta\phi$ is small results in a bias on a_1 of $-0.12 \pm 0.01\%$. The acollinearity of the τ pairs in the remaining $\gamma\tau^+\tau^-$ events yields a bias of $-0.44 \pm 0.06\%$. The bias due to errors in the measurement of θ is $+0.02 \pm 0.02\%$. The net bias due to tracking errors on d and ϕ and trimming is $+0.50 \pm 0.25\%$. The statistical uncertainty on τ_τ takes into account the small dependence of the trimming bias on τ_τ. The total uncertainty for the above biases is $\pm 0.32\%$, due to limited Monte Carlo

statistics.

The systematic uncertainty on the lifetime associated with simulation of the detector resolution is $\pm 0.26\%$. The simulation of the selection efficiency for different τ decay modes yields an uncertainty of $\pm 0.07\%$. The net lifetime bias due to backgrounds is estimated from Monte Carlo simulation to be $-0.24 \pm 0.07\%$. An additional systematic uncertainty of $\pm 0.17\%$ for the effects of final state radiation in the $Z \to \tau^+\tau^-$ decays is derived from a study of isolated photons in data and Monte Carlo. Detector alignment errors contribute $\pm 0.10\%$ to the lifetime uncertainty. The total bias is $-0.17 \pm 0.47\%$.

The mean τ lifetime is calculated from eq. 22. The mean τ momentum, $\bar{p}^0_\tau = 45.38\,\mathrm{GeV}/c$, is obtained with negligible uncertainty from a Monte Carlo simulation. The corrected a_1 corresponds to

$$\tau_\tau = 288.4 \pm 5.6\,(\mathrm{stat}) \pm 1.4\,(\mathrm{syst})\,\mathrm{fs}. \tag{23}$$

8 Decay length analysis

The classical decay length or vertex method is used to measure the mean lifetime of τ's decaying into three charged tracks.

Three-prong hemispheres with $\Sigma q = \pm 1$ are selected from the basic $\tau^+\tau^-$ sample. The event sphericity axis is determined from the reconstructed charged and neutral particles for each event containing a candidate decay. The three charged tracks are required to point within 18° of this axis. Neutral particles outside of this cone are discarded and the sphericity axis is recalculated. This procedure avoids the large τ direction error (and consequent lifetime bias) which is possible in radiative events.

Track quality cuts are applied to the three-prong candidates, as shown in table 3. In particular, each of the three tracks is required to have at least one r-ϕ or r-z hit in the VDET. Decays with an identified electron are rejected to reduce contamination from photon conversions. The decay vertex is reconstructed and fitted using the full three-dimensional information provided by the detector. A candidate is retained only if the result of the vertex fit has a χ^2 CL greater than 4%.

The position and size of the interaction region and the position and uncertainty of the fitted decay vertex are used to calculate the most probable τ flight distance; the τ flight path is constrained to be parallel to the event sphericity axis, determined as described above. The uncertainty on the τ direction is taken into account by increasing the assumed size of the interaction region in the plane perpendicular to the sphericity axis. The χ^2 CL of this decay length fit is required to be greater than 0.4%, and the uncertainty on the fitted decay length is required to be less than 0.3 cm. The typical decay length resolution is 650 μm. Figure 5 shows the decay length distribution for the remaining 2835 τ's. One τ has a fitted decay length greater than 3 cm and is discarded. The overall selection efficiency for three-prong τ decays is 30%.

The mean decay length is extracted from the decay length distribution by means of a maximum likelihood fit. The probability function is taken to be the convolution of a decreasing exponential with a Gaussian resolution function. The decay length uncertainties are multiplied by a scaling factor k which is free to vary in the fit. The results for data are $\langle \ell \rangle = 0.2209 \pm 0.0044\,\mathrm{cm}$ and $k = 1.22 \pm 0.04$. For simulated events with

Table 3: Numbers of surviving candidate τ decays in the three-prong selection.

Cut	Decays
Three prongs in cone about sphericity axis	7998
≥ 8 TPC hits	7542
≥ 1 VDET r-ϕ hit	5569
$\lvert d\rvert < 0.5\,\mathrm{cm}$; $\lvert z_0\rvert < 4\,\mathrm{cm}$	5491
$p > 0.5\,\mathrm{GeV}/c$	5388
$\Sigma(\chi^2/\mathrm{dof}) < 15$	5307
No electron	4648
Invariant mass less than $2\,\mathrm{GeV}/c^2$	4645
Vertex fit CL $> 4\%$	2893
Decay length fit CL $> 0.4\%$	2837
Decay length uncertainty $< 0.3\,\mathrm{cm}$	2836
Decay length $< 3\,\mathrm{cm}$	2835

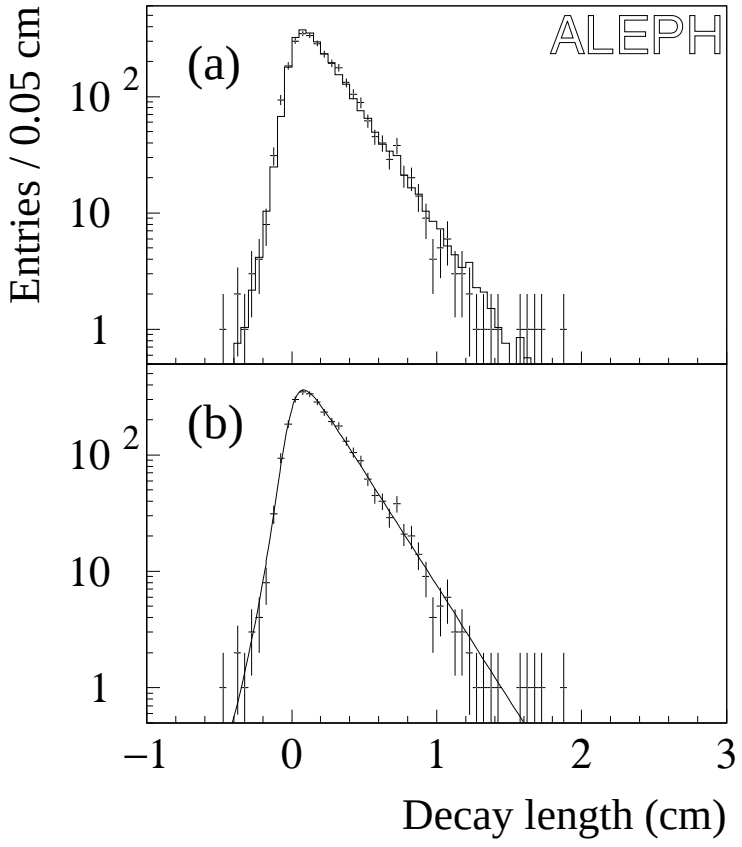

Figure 5: (a) Decay length distribution for data (squares with error bars) and Monte Carlo (histogram). The Monte Carlo decay lengths have been adjusted to correspond to $\tau_{\mathrm{mc}} = 292\,\mathrm{fs}$. (b) Decay length distribution for data with curve showing fit result.

a generated mean lifetime of 296 fs, the same procedure gives $\langle \ell \rangle = 0.2250 \pm 0.0014$ cm and $k = 1.12 \pm 0.01$. The values of k obtained from data and Monte Carlo are different because the tracking errors are smaller in the simulated events. The mean momentum of selected τ's is calculated to be 45.29 GeV/c by means of a Monte Carlo simulation. The calculated bias on the mean decay length is $-0.52 \pm 0.61\%$. This Monte Carlo result is used to correct for possible biases in the analysis.

Several sources of systematic errors are studied. First, the bias due to the residual contamination of hadronic events is found from Monte Carlo simulation to be $-0.24 \pm 0.11\%$. The effect of distortions in track z coordinate measurements, correlated with polar angle, is studied using $q\bar{q}$ events; a bias of $-0.18 \pm 0.36\%$ is found. The bias due to impact parameter offsets is zero when averaged over all azimuthal angles. The effects of pattern recognition errors are studied by varying the vertex χ^2 probability cut; a systematic uncertainty of $\pm 0.40\%$ is deduced. In order to study the tails of the tracking resolution, the decay length distribution was fitted with a two-Gaussian resolution function. The resulting amplitude of the wider Gaussian is consistent with zero, and the fitted mean decay length is identical to the value given above.

The total systematic bias and uncertainty is $-0.94 \pm 0.82\%$. The corrected τ lifetime obtained with the DL method is

$$\tau_\tau = 291.9 \pm 5.8\,(\text{stat}) \pm 2.4\,(\text{syst})\,\text{fs}. \tag{24}$$

9 Conclusions

The MIPS, IPS, and IPD analyses are all based on the 1-1 topology events. The correlation coefficients for the statistical errors of these three analyses are determined by means of a Monte Carlo simulation. The correlation coefficients are 0.84 ± 0.02 between MIPS and IPS, 0.46 ± 0.04 between MIPS and IPD, and 0.48 ± 0.04 between IPS and IPD. Some components of the systematic errors are common to two or more of the measurements. The procedure of [13] is used to determine the optimum weights for averaging the four measured lifetimes. Correlations among the statistical and systematic errors are taken into account. The combined result for the 1992 data is

$$\tau_\tau = 293.5 \pm 3.1\,(\text{stat}) \pm 1.7\,(\text{syst})\,\text{fs}, \tag{25}$$

with $\chi^2 = 2.4$ for 3 degrees of freedom (CL = 49%). Including the previous ALEPH measurements [3, 4], the combined result is

$$\tau_\tau = 293.7 \pm 2.7\,(\text{stat}) \pm 1.6\,(\text{syst})\,\text{fs}, \tag{26}$$

with $\chi^2 = 6.3$ for 10 degrees of freedom (CL = 79%). This result is consistent with the world average in [14] and with a recent measurement [15].

The ALEPH measurements of the τ lifetime and branching fractions may be used in equations 2 and 3 to test lepton universality. For $B(\tau \to e\nu\bar{\nu}) = 17.79 \pm 0.12 \pm 0.06\%$ [16], $B(\tau \to \mu\nu\bar{\nu}) = 17.31 \pm 0.11 \pm 0.05\%$ [16], $m_\tau = 1776.96 \pm 0.26\,\text{MeV}/c^2$ [5], and other quantities from [14], the ratios of the effective coupling constants are

$$\frac{g_\tau}{g_\mu} = 0.9943 \pm 0.0037(B_e) \pm 0.0053(\tau_\tau) \pm 0.0004(m_\tau) \tag{27}$$

and

$$\frac{g_\tau}{g_e} = 0.9946 \pm 0.0035(B_\mu) \pm 0.0053(\tau_\tau) \pm 0.0004(m_\tau). \quad (28)$$

These results are consistent with the hypothesis of lepton universality.

Acknowledgements

We wish to thank our colleagues in the CERN accelerator divisions for the successful operation of LEP. We are indebted to the engineers and technicians in all our institutions for their contribution to the excellent performance of ALEPH. Those of us from non-member countries thank CERN for its hospitality.

References

[1] W. Marciano and A. Sirlin, Phys. Rev. Lett. **61** (1988) 1815.

[2] K. Riles, Int. J. Mod. Phys. A **7** (1992) 7647; P.H. Chankowski, R. Hempfling, and S. Pokorski, Phys. Lett. B **333** (1994) 403.

[3] D. Decamp *et al.* (ALEPH Collaboration), Phys. Lett. B **279** (1992) 411.

[4] D. Buskulic *et al.* (ALEPH Collaboration), Phys. Lett. B **297** (1992) 432.

[5] Nading Qi (BES Collaboration), Nucl. Phys. B (Proc. Suppl.) **40** (1995) 387.

[6] D. Decamp *et al.,* Nucl. Instrum. Methods A 294 (1990) 121.

[7] G. Batignani *et al.,* conference record of the 1991 IEEE Nuclear Science Symposium (November 1991, Sante Fe, NM, USA), Vol. 1, p. 438.

[8] D. Buskulic *et al.* (ALEPH Collaboration), Z. Phys. C **62** (1994) 539.

[9] P. Abreu *et al.* (DELPHI Collaboration), Phys. Lett. B **302** (1993) 356.

[10] D. Buskulic *et al.* (ALEPH Collaboration), preprint CERN-PPE/95-023 (1995), submitted to Z. Phys. C.

[11] Computer program `KORALZ`, version 3.8, courtesy of S. Jadach, B.F.L. Ward, and Z. Wąs; S. Jadach and Z. Wąs, Comp. Phys. Commun. **36** (1985) 191; Monte Carlo Group in "Proceedings of the Workshop on Z Physics at LEP", CERN Report 89-08 (1989) Vol. III; S. Jadach, B.F.L. Ward, and Z. Wąs, Comp. Phys. Commun. **66** (1991) 276.

[12] Computer program `KORALB`; S. Jadach and Z. Wąs, Comp. Phys. Commun. **64** (1991) 267.

[13] L. Lyons, D. Gibaut, and P. Clifford, Nucl. Instrum. Methods A **270** (1988) 110.

[14] L. Montanet *et al.* (Particle Data Group), Phys. Rev. D **50** (1994) 1173.

[15] K. Abe *et al.* (SLD Collaboration), preprint SLAC-PUB-95-6767 (1995), submitted to Phys. Rev. D.

[16] D. Buskulic *et al.* (ALEPH Collaboration), preprint CERN-PPE/95-127 (1995), submitted to Z. Phys. C.